Spark plasma sintering synthesis of Ni1–xZnxFe2O4 ferrites: Mössbauer and catalytic study

Nikolay Velinov, Elina Manova, Tanya Tsoncheva, Claude Estournès, Daniela Paneva, Krassimir Tenchev, Vilma Petkova, Kremena Koleva, Boris Kunev, Ivan Mitov

Spark plasma sintering synthesis of $Ni_{1-x}Zn_xFe_2O_4$ ferrites: Mössbauer and catalytic study

Nikolay Velinov [a,*], Elina Manova [a], Tanya Tsoncheva [b], Claude Estournès [c], Daniela Paneva [a], Krassimir Tenchev [a], Vilma Petkova [d], Kremena Koleva [a], Boris Kunev [a], Ivan Mitov [a]

[a] Institute of Catalysis, Bulgarian Academy of Sciences, Acad. G. Bonchev Str., Bl. 11, Sofia 1113, Bulgaria
[b] Institute of Organic Chemistry with Centre of Phytochemistry, Bulgarian Academy of Sciences, Sofia 1113, Bulgaria
[c] CIRIMAT, CNRS - Institut Carnot, CF - 31062 Toulouse, France
[d] Institute of Mineralogy and Crystallography, Bulgarian Academy of Sciences, Sofia 1113, Bulgaria

A B S T R A C T

Nickel-zinc ferrite nanoparticles, $Ni_{1-x}Zn_xFe_2O_4$ ($x = 0, 0.2, 0.5, 0.8, 1.0$) were prepared by combination of chemical precipitation and spark plasma sintering (SPS) techniques and conventional thermal treatment of the obtained precursors. The phase composition and structural properties of the obtained materials were investigated by X-ray diffraction and Mössbauer spectroscopy and their catalytic activity in methanol decomposition was tested. A strong effect of reaction medium leading to the transformation of ferrites to a complex mixture of different iron containing phases was detected. A tendency of formation of Fe-carbide was found for the samples synthesized by SPS, while predominantly iron-nickel alloys ware registered in TS obtained samples. The catalytic activity and selectivity in methanol decomposition to CO and methane depended on the current phase composition of the obtained ferrites, which was formed by the influence of the reaction medium.

Keywords:
Nickel-zinc ferrite
Spark plasma sintering
Mössbauer spectroscopy
Methanol decomposition

1. Introduction

Spinel ferrites are widely studied due to their resistivity, mechanical hardness, remarkable stability and promising memory storage capacity. Nanosized spinel ferrites opened new prospects in biology, electronics, transport and information technology [1–7]. They are well known catalysts for dehydrogenation of hydrocarbons, decomposition of alcohols, selective oxidation of CO, hydrodesulfurization, WGSR etc. [8–11]. Ni- ferrites possess excellent activity in vapour phase oxidation of benzoic acid to phenol and catalytic decomposition of hydrogen peroxide. Superior catalytic activity of non-stoichiometric ferrites in water and carbon dioxide decomposition has been also reported recently [12,13].

The large scale of application of nanosized ferrites has promoted the development of various synthesis methods, as high energy ball-milling, hydrothermal technique, chemical co-precipitation, freeze drying, spray drying, decomposition of mixed oxides, citrates and carbonates, sonochemical preparation, sol–gel method, hydrolysis of metal carboxylate in organic solvent, etc. [14–27]. Among these available synthesis methods, spark plasma sintering was reported as the fastest synthesis technique which ensures preparation of powders with nanosize or nanostructure, avoiding coarsening, which accompanies standard densification routes [28]. It was established that the physical properties of ferrites are sensitive to method of preparation.

Spinel mixed oxides ferrites with general formula AB_2O_4, are denoted as normal spinel if all 2+ cations occupy the tetrahedral positions, and inverse spinel, if half of 3+ ions occupy tetrahedral positions and the other half and 2+ cations lie over the octahedral position. Zn and Ni are known to have a strong preference for tetrahedral and octahedral sites, respectively, making $ZnFe_2O_4$, a model of normal ferrite and $NiFe_2O_4$ a model of inverse ferrite [22]. Mixed Ni–Zn ferrites are usually denoted as $(Zn_xFe_{1-x})_{tetra}[Ni_{1-x}Fe_{1+x}]_{octa}O_4$, where the parentheses and square brackets refer to the cations occupying tetrahedral site (A site, 8 of 64 tetrahedral interstitial sites) and octahedral site (B site, 16 of 32 octahedral interstitial sites), respectively. It is known that the redistribution of metal ions over the tetrahedral and octahedral positions in the spinel lattice of these ferrites is responsible for modification of their properties [2–4].

The purpose of the present work is to investigate the possibility of synthesizing of nanocrystalline $Ni_{1-x}Zn_xFe_2O_4$ ($x = 0, 0.2, 0.5, 0.8, 1.0$) materials by spark plasma sintering (SPS) of hydroxide

* Corresponding author. Tel.: +359 29792593, fax: +359 29712967.
E-mail address: nikivelinov@ic.bas.bg (N. Velinov).

10.1016/j.solidstatesciences.2012.05.023

carbonate precursors and to compare with the structure of the materials, synthesised by conventional thermal treatment at the same temperature. To the best of our knowledge, the application of spark plasma sintering method for the preparation of nanocrystalline $Ni_{1-x}Zn_xFe_2O_4$ catalysts has not been studied yet. We tested these materials as catalysts in methanol decomposition to CO and hydrogen and investigated the changes with the spinel structure under the reaction medium. Methanol has been considered as ideal alternative green fuel for fuel cells because of its liquid state at ambient conditions and high volumetric energy density [29]. Methanol can be decomposed to CO and H_2 at relatively low temperatures, but a problem with the development of highly effective catalyst is still opened [30].

2. Experimental

2.1. Materials

Ni–Zn ferrites with composition $Ni_{1-x}Zn_xFe_2O_4$, where $x = 0$, 0.2, 0.5, 0.8, 1.0 were prepared by two methods: spark plasma sintering (SPS) and thermal synthesis (TS). The starting materials used were $Fe(NO_3)_3.9H_2O$, $Ni(NO_3)_2.6H_2O$, $Zn(NO_3)_2.6H_2O$ and Na_2CO_3. The Ni, Zn, Fe- nitrates solution was precipitated with dropwise addition of 1 M sodium carbonate solution up to pH 9 at continuous stirring. The initially obtained precipitates were dried at room temperature to form hydroxide carbonate precursor powders. The method of SPS treatment of hydroxide carbonate precursor was applied using apparatus model: SPS-2080, Sumimoto Coal Mininig Company Ltd., available at the *Plate-formae Nationale de Frittage Flash* in Toulouse, France. The following sintering parameters were used: a heating rate of 100 K/min to the final sintering temperature of 773 K and 5 min holding time; a constant pressure of 100 MPa applied before attaining the sintering temperature. The synthesis of samples by TS method was accomplished of annealing of precursor powders at 773 K for 4 h.

The samples were denoted as $Ni_{1-x}Zn_xFe_2O_4$-M, where M was the method used for the preparation of the ferrites (TS or SPS for the thermal and spark plasma sintering, respectively).

2.2. Methods of characterization

Thermogravimetry-Differential Thermal Analysis (TG-DTA) was carried out by "Stanton Redcroft" (England) apparatus in static air at 10 K/min heating rate. The powder XRD patterns were recorded by use of a TUR M62 diffractometer with Co Kα radiation. The observed patterns were cross-matched with those in the JCPDS database. The average crystallites size (D), the degree of microstrain (e) and the lattice parameters (a) of the studied ferrites were determined from the experimental XRD profiles by using the PowderCell-2.4 software [31]. The instrumental broadening of diffraction peaks is equal to 0.020° Bragg angle. It was determined by Al standard and was excluded at calculation of crystallites size and the degree of microstrain. The Mössbauer spectra were obtained at room temperature (RT) with a Wissel (Wissenschaftliche Elektronik GmbH, Germany) electromechanical spectrometer working in a constant acceleration mode. A $^{57}Co/Cr$ (activity ≅10 mCi) source and a α-Fe standard were used. The experimentally obtained spectra were fitted to mathematical processing according to the least squares method. The parameters of hyperfine interaction such as isomer shift (IS), quadrupole splitting (QS), effective internal magnetic field (Heff), line widths (FWHM), and relative weight (G) of the partial components in the spectra were determined. Temperature-programmed reduction (TPR) of the samples was carried out in the measurement cell of a differential scanning calorimeter (DSC-111, SETARAM) directly connected to a gas chromatograph (GC). Measurements were made in the 300–973 K range at 10 K/min heating rate in a flow of Ar:H_2 = 9:1, the total flow rate being 20 ml/min. A cooling trap between DSC and GC removes the water obtained during the reduction.

2.3. Catalytic experiments

Methanol conversion was carried out in a flow reactor (0.055 g of catalyst, three times diluted with grounded glass), argon being used as a carrier gas (50 ml/min). The methanol partial pressure was 1.57 kPa. The catalysts were tested under conditions of a temperature-programmed regime within the range of 350–770 K with heating rate of 1 K/min. On-line gas chromatographic analyses were performed on HP apparatus equipped with flame ionization and thermo-conductivity detectors, on a PLOT Q column, using an absolute calibration method and a carbon based material balance. The products selectivity was calculated as Xi/X*100, where Xi is the current yield of the product i and X is methanol conversion.

3. Results and discussion

TG-DTA analyses were carried out to investigate the thermal evolution of the hydroxide carbonate precursors and formation of $ZnFe_2O_4$, $Ni_{0.5}Zn_{0.5}Fe_2O_4$ and $NiFe_2O_4$ ferrite phases. The DTA curves of the samples (not shown) consist of several thermal effects. The endothermal effects are accompanied with a mass loss and could be assigned to precursors dehydration and decarbonisation. The exothermal effects appearing at higher temperature are not accompanied with mass loss and could be associated with formation of Ni–Zn ferrite phase. The maxima of exothermal effects are at 748 K and 823 K for $ZnFe_2O_4$ and $NiFe_2O_4$, respectively. Two weakly expressed effects with maxima at 723 K and 783 K are observed for $Ni_{0.5}Zn_{0.5}Fe_2O_4$. No additional thermal effects are observed after the exothermal effects indicating that the spinel phase formation has been completed at corresponding temperatures. Taking into account the heating rate during the DTA analysis, it has been assumed that the temperature of 773 K is the minimal required one for the thermal synthesis of Ni–Zn ferrites from obtained precipitated precursors.

X-ray powder diffraction patterns of all materials consist of peaks, demonstrating formation of single $Ni_{1-x}Zn_xFe_2O_4$ ferrite phase (Fig. 1). The average crystallites size (D), the degree of microstrain (e) and the lattice parameters (a) are presented in Table 1. The crystallite size decreases from 28.7 to 19.3 nm with the increase of Ni content in the ferrites obtained by the TS method. The samples synthesized by the SPS technique have slightly lower crystallite size than the thermally synthesized samples, but without well expressed correlation between the Zn content and crystallite size. Increasing the Zn concentration, the lattice parameters increase from 8.332 to 8.432 Å and from 8.340 to 8.433 Å for the TS and SPS synthesized materials, respectively. This expansion of lattice is expected due to the substitution of Ni^{2+} ions with larger Zn^{2+} ions [23]. The microstrain indexes demonstrate higher values for the corresponding SPS materials indicating higher defective crystal structure in this case.

Room-temperature Mössbauer spectra of the investigated samples are presented in Fig. 2. The best parameters of the fits of the Mössbauer spectra are given in Table 2. In the $ZnFe_2O_4$ ferrite the tetrahedral (A) sites are occupied by only one type of cations. This is because of the preferences of Zn^{2+} to occupy the tetrahedral spinel sites forming normal spinel, while Ni^{2+} occupies mainly the octahedral [B] sites, and thus, the tetrahedral sites are occupied by half of Fe^{3+} and $NiFe_2O_4$ describes as fully inverse spinel. In the case of $Ni_{1-x}Zn_xFe_2O_4$, where $0 < x < 1$, the tetrahedral sites are

occupied both by Zn^{2+} and Fe^{3+} cations. As it is known in spinel ferrites the dominant magnetic super exchange interaction is (A)-O-[B], which is typically 15–20 times stronger than the [B]-O-[B] interaction [32]. This is expressed in Mössbauer spectra of $NiFe_2O_4$ samples (Table 2) that were well fitted by two sextets with parameters typical of Fe^{3+} ions in octahedral and Fe^{3+} ions in tetrahedral coordination [33]. In the case of $x = 0.2$ and 0.5, it is seen that acceptable data fitting could be obtained only when the octahedral [B]-site pattern is assumed to be a superposition of more than one sextet. This is caused by the random occupancy of the tetrahedral site by Fe^{3+} and diamagnetic Zn^{2+} and consequently, results in appearance of different nearest (A)-site neighbours to Fe^{3+} ions on the [B]-site, i.e. Fe^{3+} [B]-site ion has 6Fe, 5 Fe and 1 Zn, 4 Fe and 2 Zn and etc. neighbours (corresponding sextet components are denoted in Table 2 as B0, B1, B2 and etc. respectively). The probability P(n,x) of an octahedral site having *n* nearest-neighbour zinc atoms was calculated using the binomial formula in order to define the number of sextet components that have to use in the fitting model. The components with P(n,x) lower than 2% have very small contributions in the Mössbauer spectra and was omitted. The calculated probability for the samples with Zn content of $x = 0.8$ for presence of 4 Zn^{2+} neighbours is not negligible and $P(4,0.8) = 0.25$, but the Mössbauer spectral effects of the samples with this chemical composition, prepared by both TS and SPS methods, are characterized with absence of hyperfine magnetic interaction. The Mössbauer spectra of the samples prepared by TS and SPS methods are similar, but the ones corresponding to the TS obtained materials exhibit lower values of the hyperfine magnetic fields than those observed for the SPS series.

The TPR profiles of SPS and TS obtained materials are presented at Fig. 3. For all materials the reduction transitions start around 523–573 K and they are completed around 900–973 K. The TPR profiles of all samples are broad and they could be considered as a superposition of reduction transitions of Ni^{2+}, Fe^{3+} and Zn^{2+} ions. It is known that the reduction of pure Fe_2O_3 is a stepwise process and it converts to Fe_3O_4, further to FeO and finally to Fe^0 [8]. The position of the temperature maxima may vary from sample to sample depending on the particle size. Note that the TPR profiles of TS obtained materials differ in their shape in comparison with the corresponding SPS ones. The profiles of TS materials are broadening to lower temperatures, which indicates easier reduction, the effect being most pronounced for the nickel-rich materials.

In Figs. 4 and 5 are demonstrated the catalytic activity and products distribution (presented as CO selectivity) in methanol decomposition for both series of ferrites, prepared by different methods. The samples, obtained by thermal synthesis (Fig. 4) exhibit catalytic activity above 500 K and in a narrow temperature interval (580–600 K) about 100% conversion is achieved. The bi-component ferrites present higher catalytic activity in comparison with the mono-component ones, especially when $x = 0.5$. The main carbon containing product of methanol decomposition is CO, but methane (1–20%) and CO_2 (10–30%) in different yields,

Table 1
Average crystallites size (D), degree of microstrain (e) and lattice parameters (a) determined from the experimental XRD profiles.

Sample	D, nm	e. 10^3, a.u	A, Å
$ZnFe_2O_4$-TS	28.67	0.227	8.432
$Ni_{0.2}Zn_{0.8}Fe_2O_4$-TS	26.00	0.427	8.416
$Ni_{0.5}Zn_{0.5}Fe_2O_4$-TS	24.60	0.646	8.387
$Ni_{0.8}Zn_{0.2}Fe_2O_4$-TS	19.34	1.233	8.363
$NiFe_2O_4$-TS	19.30	1.599	8.332
$ZnFe_2O_4$–SPS	22.27	1.145	8.433
$Ni_{0.2}Zn_{0.8}Fe_2O_4$-SPS	20.46	1.886	8.414
$Ni_{0.5}Zn_{0.5}Fe_2O_4$-SPS	28.46	0.881	8.397
$Ni_{0.8}Zn_{0.2}Fe_2O_4$-SPS	15.84	1.497	8.350
$NiFe_2O_4$-SPS	18.18	2.071	8.340

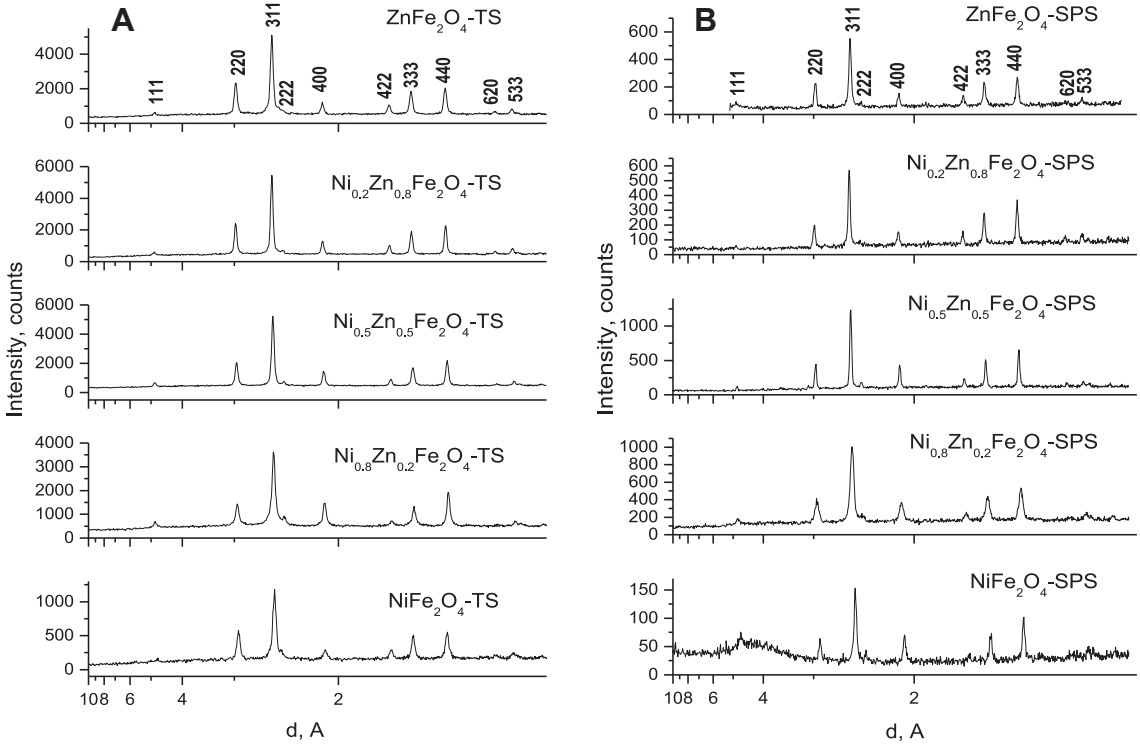

Fig. 1. X-ray diffraction patterns of (A)thermally synthesized and (B) SPS samples.

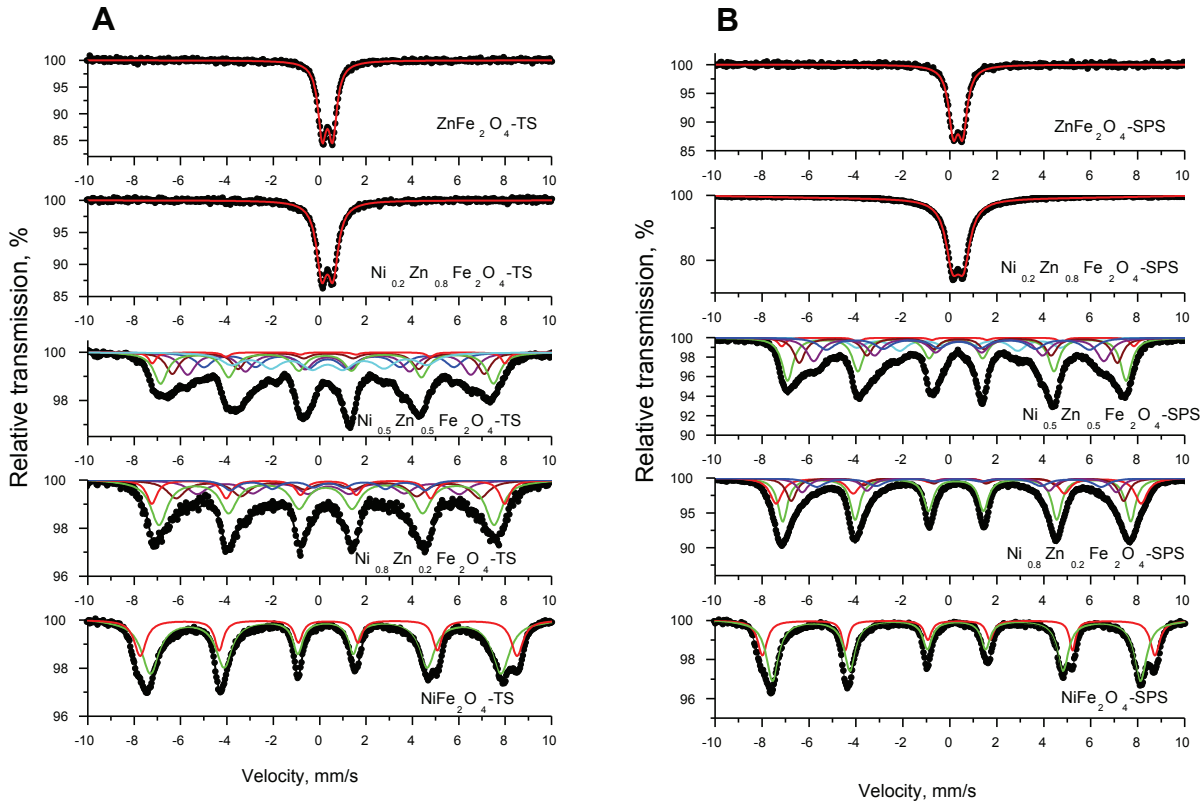

Fig. 2. Mössbauer spectra of (A) TS and (B) SPS obtained samples.

depending on the samples composition are registered, as well. The yields of by-products vary with the reaction temperature, being maximal between 590 and 630 K. Again, the highest selectivity to CO is registered for $Ni_{0.5}Zn_{0.5}Fe_2O_4$-TS, while the selectivity to CH_4 and CO_2 formation increases significantly when $x = 0$. The observed relation between the samples composition and their catalytic behaviour are not confirmed for the SPS obtained materials (Fig. 5). All bi-component ferrites from this series exhibit catalytic activity

Table 2
Parameters of Mössbauer spectra of the investigated samples.

Sample	Components	IS, mm/s	QS, mm/s	H_{eff}, T	FWHM, mm/s	G, %
$ZnFe_2O_4$-TS	Db	0.34	0.45	–	0.47	100
$Ni_{0.2}Zn_{0.8}Fe_2O_4$-TS	Db	0.33	0.49	–	0.55	100
$Ni_{0.5}Zn_{0.5}Fe_2O_4$-TS	Sx1-tetra, A	0.28	0.04	44.7	0.70	25
	Sx2-octa, B1 (0.09)	0.38	0.01	47.3	0.38	3
	Sx3-octa, B2 (0.23)	0.38	0.00	41.8	0.67	14
	Sx4-octa, B3 (0.31)	0.38	0.04	38.0	0.79	21
	Sx5-octa, B4 (0.23)	0.38	0.02	33.5	0.88	18
	Sx6-octa, B5 (0.09)	0.38	0.03	26.2	1.06	19
$Ni_{0.8}Zn_{0.2}Fe_2O_4$-TS	Sx1-tetra, A	0.28	0.02	44.9	0.87	42
	Sx2-octa, B0 (0.26)	0.38	0.00	47.3	0.54	14
	Sx3-octa, B1 (0.39)	0.38	−0.02	40.7	0.95	19
	Sx4-octa, B2 (0.25)	0.38	−0.01	35.1	0.98	17
	Sx5-octa, B3 (0.08)	0.38	−0.02	26.1	0.71	8
$NiFe_2O_4$-TS	Sx1-tetra, A	0.26	0.00	47.0	0.84	70
	Sx2-octa, B0	0.38	0.00	50.6	0.51	30
$ZnFe_2O_4$-SPS	Db	0.34	0.40		0.47	100
$Ni_{0.2}Zn_{0.8}Fe_2O_4$-SPS	Db	0.34	0.47		0.68	100
$Ni_{0.5}Zn_{0.5}Fe_2O_4$-SPS	Sx1-tetra, A	0.28	0.01	44.8	0.57	30
	Sx2-octa, B1 (0.09)	0.38	−0.04	46.9	0.39	3
	Sx3-octa, B2 (0.23)	0.38	−0.01	42.1	0.57	17
	Sx4-octa, B3 (0.31)	0.38	0.00	38.4	0.73	22
	Sx5-octa, B4 (0.23)	0.38	−0.03	34.8	0.86	15
	Sx6-octa, B5 (0.09)	0.38	0.00	26.9	0.82	12
$Ni_{0.8}Zn_{0.2}Fe_2O_4$-SPS	Sx1-tetra, A	0.28	0.01	48.3	0.63	42
	Sx2-octa, B0 (0.26)	0.38	−0.01	46.1	0.51	20
	Sx3-octa, B1 (0.39)	0.38	−0.05	44.0	0.53	13
	Sx4-octa, B2 (0.25)	0.38	0.03	41.6	0.59	13
	Sx5-octa, B3 (0.08)	0.38	0.01	37.7	0.85	12
$NiFe_2O_4$-SPS	Sx1-tetra, A	0.28	0.00	48.7	0.52	71
	Sx2-octa, B0	0.38	0.00	52.0	0.41	29

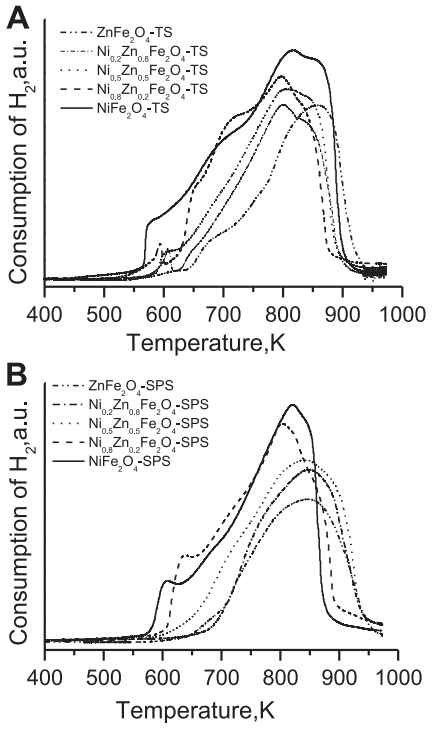

Fig. 3. TPR profiles of TS (A) and SPS (B) obtained samples.

above 550 K, which is slightly lower in comparison with their TS obtained analogues. Again, the highest activity is demonstrated for the $Ni_{0.5}Zn_{0.5}Fe_2O_4$-SPS sample, but the selectivity to CO formation on it is lower. We should stress on the extremely high activity for both mono-component SPS obtained ferrites (Fig. 5). Their conversion curves are shifted with about 150 K to the lower temperatures and at 500 K a complete decomposition of methanol with about 100% selectivity to CO is observed.

We followed the changes with the catalysts after the catalytic test by XRD and Mössbauer spectroscopy (Figs. 6 and 7, Table 3). XRD data clearly show presence of ZnO phase for all Zn-containing ferrites after catalysis. The parameters of the doublet components in the Mössbauer spectra of $ZnFe_2O_4$-TS (Fig. 7, Table 3) confirm the appearance of (Fe,Zn) alloy [42]. A mixture of different iron containing phases, such as α- and γ- (Fe, Ni) alloys, Fe_3C, wuestite and magnetite in different proportion was detected in all spectra. The presence of γ- (Fe, Ni) alloy is registered by Mössbauer spectroscopy as sextet with parameters typical of the fcc ferromagnetic chemically disordered taenite phase and a single line with IS between −0.06 and −0.02 mm/s can be attributed to a fcc iron rich paramagnetic phase that usually coexist with the ferromagnetic one [43]. A clear tendency of formation of Fe-carbide is observed for the samples synthesized by SPS, while iron-nickel alloy is mainly registered in thermally obtained samples. Significant amount of FeO (G = 50%) and Fe_3O_4 (G = 32%) iron oxide phases are also registered for the mono-component Zn- and Ni- TS obtained materials, respectively. We would like also to stress on the step wise evolution of active phase during the catalytic process. According to [41], under relatively mild reduction conditions, which realizes in a narrow temperature interval, low hydrogen rate and short reduction time, only partial reduction of ferrite with the appearance of small oxygen deficit and preservation of the spinel structure occurs. It was also reported the extremely high activity of these O-deficient ferrites in reactions of

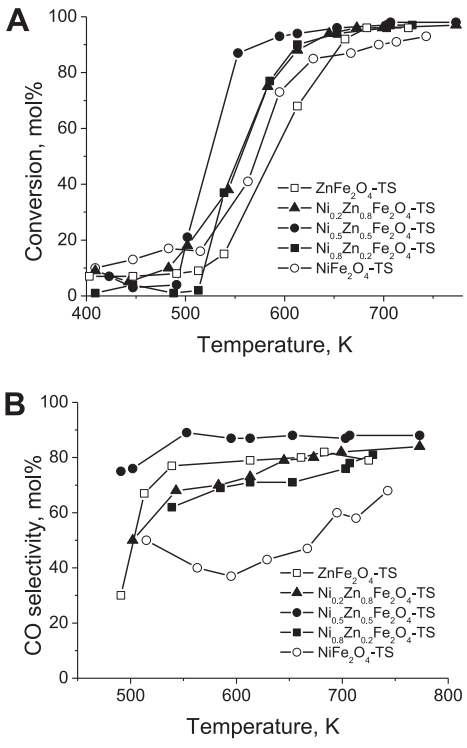

Fig. 4. Methanol conversion (A) and CO selectivity (B) vs. temperature of materials synthesized by TS method.

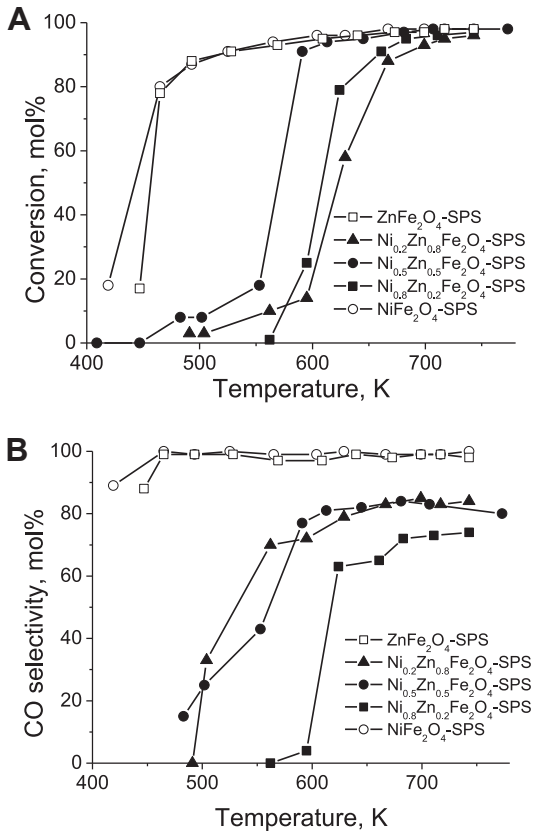

Fig. 5. Methanol conversion (A) and CO selectivity (B) vs. temperature of materials synthesized by SPS method.

decomposition of various compounds (H_2O, CO_2) [41]. Under the experimental conditions with the increase of the reaction temperature, the amount of reducing reagents (H_2, CO) and prolonging the time of reduction, destructive changes with the spinel structure with the formation of metal α-Fe and FeNi alloy occur. These phases could be transformed further after the reaction with the products of methanol decomposition, such as CO_2, CO and H_2O, with the formation of magnetite and iron carbide. Taking into account that each of these phases possesses its own catalytic performance, we assume that the catalytic behaviour of the samples depends on the current phase composition, which is a complex mixture of initial spinel sample and its derivates formed by the influence of reaction medium. It is known that the decrease in the particles size leads also to the appearance of defect spinel structure. We confirmed the formation of defect spinel structure by the calculated degree of microstrain of the lattice (Table 1). It increases with the increase of nickel content in the samples, being the larger for the SPS obtained materials. According to [39], the formation of defects includes a creation of oxygen vacancies, inducing surface spin disorder or leads to occupation of normally unoccupied sites by ferric ions. A size dependent effect was also reported in ref. [40], where cation inversion increase with particle size decrease was observed for Zn-ferrite. We expect that the changes in the ions environment in these defective structures provide more complex relation between the catalytic activity and samples composition.

We could not ignore also the effect of ions distribution in the initial spinel lattice on their catalytic behaviour. For the mono-component ferrites, a preference occupation of tetrahedral and octahedral positions of the spinel with Zn and Ni ions, respectively,

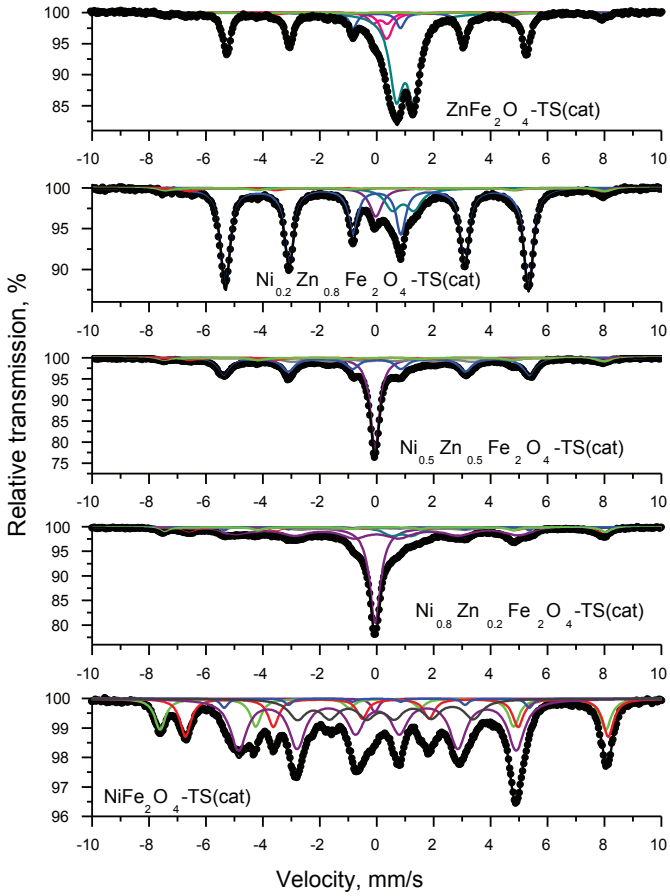

Fig. 6. Mössbauer spectra of TS samples after catalytic test.

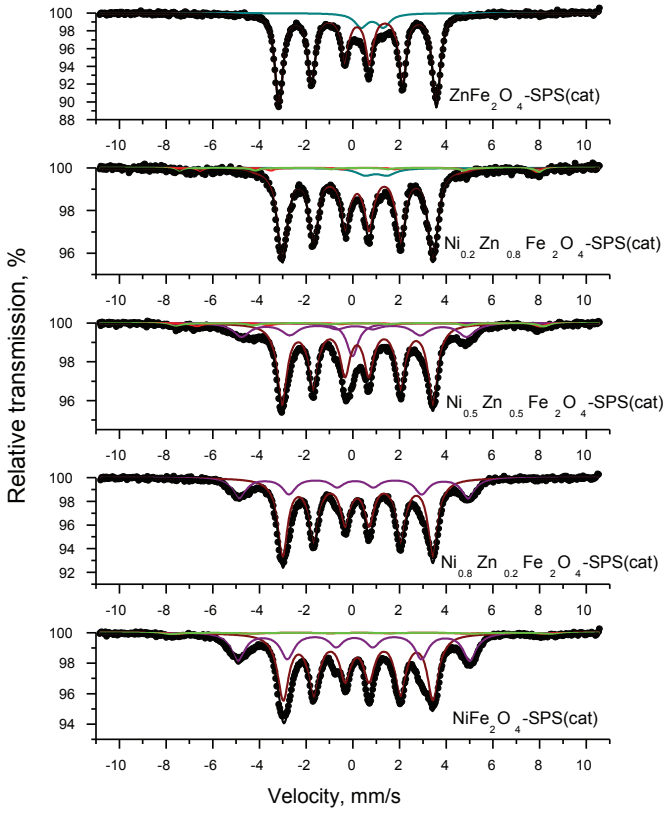

Fig. 7. Mössbauer spectra of SPS samples after catalytic test.

is generally reported [8,22,23,34,35]. This tendency is related to the electronic configuration of Zn^{2+} ions with free 4s4p orbitals, which are ready to form covalent bonds with oxygen ions, when the Zn ions occupy the (A) sites only, while the high crystal field stabilization energy of Ni^{2+} ions leads to their predominant situation on [B] sites of the spinel lattice. On increase of the Zn concentration upon (A) site in bi-component ferrites, the concentration of Ni ions upon the [B] site should be decreased. This leads to the migration of iron ions from (A) site to [B] site. As a result the number of ferric ions at [B] site increases and during the redox catalytic process more intensive electron exchange between them is expected [36,37]. According to [22], the catalytic sites in spinel type structure could be related to the redox pairs of metal ions in different valence state on equivalent (octahedral) position. In the case of Ni-ferrite materials they are $Fe^{3+} \leftrightarrow Fe^{2+}$ redox pairs [8,38]. Electron transfer between different metal ions type $Ni^{2+} + Fe^{3+} \leftrightarrow Ni^{3+} + Fe^{2+}$ is not excluded as well. We expect that the electron transfer in these couple of ions depends on their local environment. We demonstrated the probability of Fe ions in octahedral positions to have 0, 1, 2 etc. Zn neighbours, situated on tetrahedral sites (Table 2), which depends both on the samples composition and the preparation method used. We suggest that the situation of the Zn ions in the vicinity of the $Fe^{3+} \leftrightarrow Fe^{2+}$ redox centres could intensify the electron transfer in them due to the lower electronegativity of Zn ions in comparison with the Fe ones. This is the case of the materials obtained by the TS method as well as of the samples with $Ni_{0.5}Zn_{0.5}Fe_2O_4$ composition despite the method of preparation, where higher catalytic activity is detected (Figs. 4 and 5). The above presented explanations would have greater importance in cases of lower temperatures, at which the ferrite-spinel structure is not altered yet. At the higher temperatures the mechanism of the catalytic reaction is changing and the higher degree of conversion of methanol to hydrogen and CO is probably determined by the metal-carbide phases.

In conclusion, the catalytic effects depend in a complex way on the initial state of ferrites, due to intensive changes with their composition by the influence of reaction medium. The clear relations between the current catalyst composition and its behaviour could be found using in situ measurements and further investigations are in progress.

4. Conclusions

In this work it has been demonstrated that the method of spark plasma sintering of nickel-zinc-iron hydroxide carbonate precursors results in the formation of nanocrystalline Ni–Zn ferrites. The structural and magnetic properties of the samples exhibit a strong dependence on the chemical composition. Mössbauer spectra of the samples after methanol decomposition demonstrate significant changes in the phase composition due to the influence of the reaction medium. A complex mixture of iron containing phases as α- and γ- (Fe, Ni) alloys, Fe_3C, wuestite and magnetite in different proportion are detected. A tendency of formation of Fe-carbide is found for samples synthesized by SPS, while iron-nickel alloy is mainly registered in thermally obtained samples. The final catalytic behaviour of the samples depends on their current phase composition, which is determined on the initial distribution of ions in the spinel lattice and their flexibility under the reduction reaction medium. The highest activity and selectivity to CO formation is observed for mono-component ferrites obtained by SPS technique.

Table 3
Parameters of Mössbauer spectra of the investigated samples after catalytic reaction of methanol decomposition.

Sample	Components	IS, mm/s	QS, mm/s	H_{eff}, T	FWHM, mm/s	G, %
$ZnFe_2O_4$-TS(cat)	Sx1-Fe_3O_4, Fe^{3+}tetra	0.29	−0.02	48.1	0.50	3
	Sx2-Fe_3O_4, $Fe^{2.5+}$octa	0.67	0.00	45.1	0.50	3
	Sx3-α-Fe, Fe^0	0.00	−0.03	32.8	0.33	33
	Db1-FeO, Fe^{2+}	1.00	0.62	–	0.56	50
	Db2-Γ-(Fe,Zn)-A, Fe^0	0.35	0.16	–	0.40	7
	Db3-Γ-(Fe,Zn)-B, Fe^0	0.12	0.50	–	0.40	4
$Ni_{0.2}Zn_{0.8}Fe_2O_4$-TS(cat)	Sx1-Fe_3O_4, Fe^{3+}tetra	0.29	0.00	48.1	0.60	3
	Sx2-Fe_3O_4, $Fe^{2.5+}$octa	0.67	0.00	45.1	0.60	3
	Sx3-α-Fe, Fe^0	0.00	0.00	33.1	0.40	72
	Db-FeO, Fe^{2+}	0.93	0.76	–	0.63	10
	Sn-γ-(Fe, Ni) alloy, Fe^0	−0.03	–	–	0.51	12
$Ni_{0.5}Zn_{0.5}Fe_2O_4$-TS(cat)	Sx1-Fe_3O_4, Fe^{3+}tetra	0.29	−0.02	48.1	0.60	7
	Sx2-Fe_3O_4, $Fe^{2.5}$octa	0.67	0.00	45.1	0.60	7
	Sx3-α-Fe, Fe^0	0.00	0.00	33.4	0.55	40
	Sx4-Fe_3C, Fe^0	0.19	0.01	19.7	0.86	14
	Sn-γ-(Fe, Ni) alloy, Fe^0	−0.06	–	–	0.38	32
$Ni_{0.8}Zn_{0.2}Fe_2O_4$-TS(cat)	Sx1- Fe_3O_4, Fe^{3+}tetra	0.30	−0.02	48.1	0.40	5
	Sx2- Fe_3O_4, $Fe^{2.5+}$octa	0.67	0.00	45.1	0.56	8
	Sx3- α-(Fe, Ni) alloy, Fe^0	0.00	0.00	33.3	0.22	3
	Sx4- γ-(Fe, Ni) alloy, Fe^0	0.00	0.00	30.8	1.13	39
	Sx5-Fe_3C, Fe^0	0.19	0.01	17.9	0.89	6
	Db-FeO, Fe^{2+}	0.88	0.72	–	0.70	7
	Sn-γ-(Fe, Ni) alloy, Fe^0	−0.06	–	–	0.46	32
$NiFe_2O_4$-TS(cat)	Sx1-Fe_3O_4, Fe^{3+}tetra	0.30	−0.02	49.0	0.45	14
	Sx2-Fe_3O_4, $Fe^{2.5}$octa	0.65	0.00	45.9	0.43	18
	Sx3-α-(Fe, Ni) alloy, Fe^0	0.00	0.00	33.3	0.31	2
	Sx4-γ-(Fe, Ni) alloy, Fe^0	0.02	−0.02	30.2	0.76	47
	Sx5-Fe_3C, Fe^0	0.20	0.01	19.2	0.66	17
	Sn-γ-(Fe, Ni) alloy, Fe^0	−0.04	–	–	0.34	2
$ZnFe_2O_4$-SPS(cat)	Sx-Fe_3C, Fe^0	0.19	0.01	20.9	0.40	90
	Db-FeO, Fe^{2+}	0.83	0.96	–	0.66	10
$Ni_{0.2}Zn_{0.8}Fe_2O_4$-SPS(cat)	Sx1-Fe_3O_4, Fe^{3+}tetra	0.28	0.00	47.9	0.40	2
	Sx2-Fe_3O_4, $Fe^{2.5+}$octa	0.66	0.00	44.8	0.40	3
	Sx3-Fe_3C, Fe^0	0.20	0.01	20.0	0.51	90
	Db-FeO, Fe^{2+}	0.99	0.94	–	0.90	5
$Ni_{0.5}Zn_{0.5}Fe_2O_4$-SPS(cat)	Sx1-Fe_3O_4, Fe^{3+}tetra	0.29	0.00	48.9	0.60	3
	Sx2-Fe_3O_4, $Fe^{2.5+}$octa	0.67	0.00	45.7	0.60	3
	Sx3- γ-(Fe, Ni) alloy, Fe^0	0.07	−0.02	30.0	0.86	18
	Sx4-Fe_3C, Fe^0	0.19	0.01	20.1	0.51	69
	Sn-γ-(Fe, Ni) alloy, Fe^0	−0.02	–	–	0.59	7
$Ni_{0.8}Zn_{0.2}Fe_2O_4$-SPS(cat)	Sx1- γ-(Fe, Ni) alloy, Fe^0	0.07	−0.03	30.5	0.69	25
	Sx2-Fe_3C, Fe^0	0.19	0.01	20.0	0.52	75
$NiFe_2O_4$-SPS(cat)	Sx1-$NiFe_2O_4$, Fe^{3+}octa	0.38	0.00	51.0	0.85	1
	Sx2-$NiFe_2O_4$, Fe^{3+}tetra	0.28	0.00	48.9	0.85	2
	Sx3-γ-(Fe, Ni) alloy, Fe^0	0.06	−0.01	30.8	0.70	31
	Sx4-Fe_3C, Fe^0	0.21	0.032	19.9	0.58	66

Acknowledgement

Sponsorship by Bulgarian National Science Fund at the Ministry of Education, Youth and Science under DO 02-295/2008 is gratefully acknowledged.

References

[1] M. Pardavi-Horvath, J. Magn. Magn. Mater. 215-216 (2000) 171–183.
[2] E. Manova, B. Kunev, D. Paneva, I. Mitov, L. Petrov, C. Estournès, C. D'Orléans, J.-L. Rehspringer, M. Kurmoo, Chem. Mater. 16 (2004) 5689–5696.
[3] E. Manova, D. Paneva, B. Kunev, E. Rivière, C. Estournès, I. Mitov, J. Phys. Conf. Ser. 217 (2010) art. no. 012102.
[4] E. Manova, T. Tsoncheva, Cl. Estournès, D. Paneva, K. Tenchev, I. Mitov, L. Petrov, Appl. Catal. A 300 (2006) 170–180.
[5] T. Tsoncheva, E. Manova, N. Velinov, D. Paneva, M. Popova, B. Kunev, K. Tenchev, I. Mitov, Catal. Commun. 12 (2010) 105–109.
[6] A. Goldman, in: L. Levenson (Ed.), Electronic Ceramics, Marcel Dekker, New York, 1988.
[7] J.L. Dormann, D. Fiorani, Magnetic Properties of Fine Particles (1992) North-Holland, Amsterdam.
[8] A. Khan, P.G. Smirniotis, J. Mol. Catal. A: Chem. 280 (2008) 43–51.
[9] J. Miki, M. Asanuma, Y. Tachibana, T. Shikada, Appl.Catal. A: Gen. 143 (1996) 215–222.
[10] J. Miki, M. Asanuma, Y. Tachibana, T. Shikada, J. Catal. 151 (1995) 323–330.
[11] S.K. Mazumdar, A.S. Brar, Thermochim. Acta 93 (1985) 505–508.
[12] K.-S. Lin, A. K. Adhikari, Z.-Y.Tsai, Y.-P. Chen, T.-T. Chien, H.-B.Tsai, Catal. Today, doi:10.1016/j.cattod.2011.02.013.
[13] Y. Tamaura, M. Tabata, Nature 346 (1990) 255–256.
[14] S. Gin, S. Samanta, S. Maji, S. Gangli, J. Magn. Magn. Mater. 288 (2005) 296–302.
[15] G.R. Dube, V.S. Darshane, J. Mol. Catal. 79 (1993) 285–296.
[16] C. Upadhay, H.C. Verma, S. Anand, J. Phys. 95 (2004) 5746–5751.
[17] R.D. Shannon, C.T. Prewitt, Acta Cryst. B26 (1970) 1046–1048.
[18] Y. Shi, J. Ding, X. Liu, J. Wang, J. Magn. Magn. Mater. 205 (1999) 249–254.
[19] X. Yi, Q. Yitai, L. Jing, C. Zuyao, Y. Li, Mater. Sci. Eng. B 34 (1995) L1–L3.
[20] M.M. Bucko, K. Haberko, J. Eur. Ceram. Soc. 27 (2007) 723–727.
[21] A. Kumar, Annveer, M. Arora, M.S. Yadav, R.P. Pant, Phys. Proced. 9 (2010) 20–23.
[22] I.H. Gul, W. Ahmed, A. Maqsoo, J. Magn. Magn. Mater. 320 (2008) 270–275.
[23] P.P. Hankare, U.B. Sankpal, R.P. Patil, I.S. Mulla, R. Sasikala, A.K. Tripathi, K.M. Garadkar, J. Alloys Comp. 496 (2010) 256–260.
[24] V. Sepelak, D. Baabe, D. Mienert, D. Schultze, F. Krumeich, F.J. Litterst, K.D. Beckera, J. Magn. Magn. Mater. 257 (2003) 377–386.
[25] R. Malik, S. Annapoorni, S. Lamba, V.R. Reddy, A. Gupta, P. Sharmad, A. Inoue, J. Magn. Magn. Mater. 322 (2010) 3742–3747.
[26] M. Atif, M. Nadeem, R. Grössinger, R. Sato Turtelli, J. Alloys Comp. 509 (2011) 5720–5724.
[27] M. Srivastav, S. Chaubey, Animesh K. Ojh, Mater. Chem. Phys. 118 (2009) 174–180.
[28] N. Millot, S. Le Gallet, D. Aymes, F. Bernard, Y. Grin, J. Eur. Ceram. Soc. 27 (2007) 921–926.
[29] M.S. Wilson, Int. J. Hydrogen Energy 34 (2009) 2955–2964.

[30] M. Manzoli, A. Chiorino, F. Boccuzzi, Appl. Catal. B: Environ. 57 (2005) 201–209.
[31] W. Kraus, G. Nolze, PowderCell for Windows, Federal Institute for Materials Research and Testing, Berlin, 2000.
[32] P.J. van der Zaag, in: K.H.J. Buschow (Ed.), Concise Encyclopedia of Magnetic and Superconducting Materials, second ed., Elsevier, The Netherlands, 2005, pp. 179–183.
[33] M. Sorescu, L. Diamandescu, R. Peelamedu, R. Roy, P. Yadoji, J. Magn. Magn. Mater. 279 (2004) 195–201.
[34] P.A. Joy, S.K. Date, J. Magn. Magn. Mater. 218 (2000) 229–237.
[35] M. Ajmal, A. Maqsoo, Mater. Sci. Eng. B 139 (2007) 164–170.
[36] R.J. Rennard, W.L. Kehl, J. Catal. 21 (1971) 282–293.
[37] D.G. Reithwisch, J.A. Dumesic, Appl. Catal. 97 (1986) 109–116.
[38] Z. Cherkezova-Zheleva, I. Mitov, J. Phys. Conf. Ser. 217 (2010) 012044.
[39] H. Nathani, S. Gubbala, R.D.K. Misra, Mater. Sci. Eng. B 121 (2005) 126–136.
[40] A. Verma, O.P. Thakur, C. Prakash, T.C. Goel, R.G. Mendiratta, Mater. Sci. Eng. B 116 (2005) 1.
[41] G.S. Shahane, A. Kumar, M. Arora, R.P. Pant, K. Lal, J. Magn. Magn. Mater. 322 (2010) 1015–1019.
[42] R.G. Grant, D.C. Cook, Hyperfine Interact. 94 (1994) 2309–2315.
[43] E. Lima Jr., V. Drago, R. Bolsoni, F.P. Paulo, Solid State Commun. 125 (2003) 265–270.